Optica Applicata, Vol. X, No. 4, 1980

Letters to the Editor

Extension of finite periodic object image by a partial elimination of information

Andrzej Kalestyński

Institute of Physics, Technical University of Warsaw, Warsaw, Poland.

Sometimes in optical data processing we intend to obtain a periodic signal extended over a large area.

Selected spatial filtration used in this paper is based on the properly matched mascaring. Image extending involves the elimination of a selected part of information concerning optical object dimensions. In the case of periodic signals this part obviously must be periodically deleted. Now we want to lose the information about finite periodic object dimensions in Fourier image and in this manner to obtain the infiniteness of the image (fig. 1).

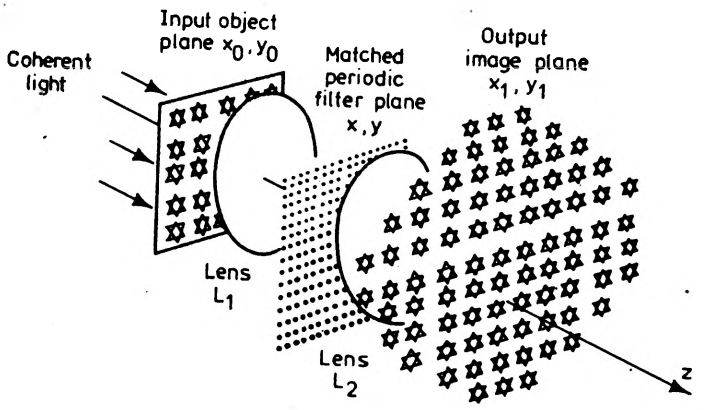

Fig. 1. Scheme of coherent optical system

Transmittance of a finite periodic object is

$$t_{\text{fin}} = t_c(x_0, y_0) \otimes \sum_{m=-M}^{m=+M} \sum_{n=-N}^{n=+N} \delta(x_0 - m d_{x_0}, y_0 - n d_{y_0}), \tag{1}$$

and its Fourier image:

$$F\{t_{\text{fin}}\} = F\{t_c\} \frac{\sin 2\pi (M+1) d_{x_0} x}{\sin 2\pi d_{x_0} x} \times \frac{\sin 2\pi (N+1) d_{y_0} y}{\sin 2\pi d_{y_0} y}, \tag{2}$$

where $F\{\ \}$ — Fourier operator, $\otimes$ — convolution symbol.

For the sake of simplicity we assume that the object, placed at focal distance before the lens, is transilluminated by normally incident plane wave, where $\hat{U}_0 = U_0 \exp(ikz)$, $k = \frac{2\pi}{\lambda}$. One-dimensional diagrams of these functions are shown in fig. 2.

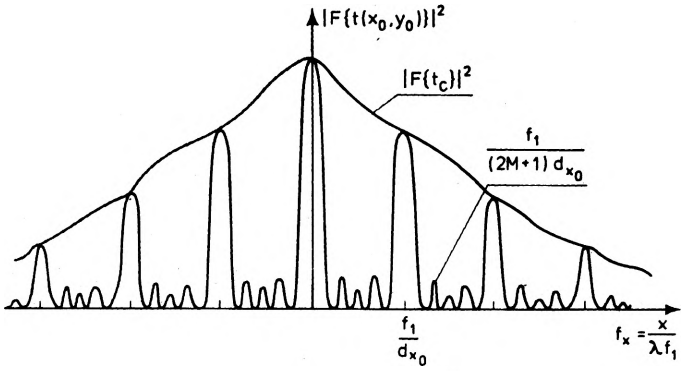

Fig. 2. Diagram of the Fourier spectrum of a finite periodic object

Fourier image (fig. 2) of t_{fin} contains a series of little peaks caused by finite dimensions of the periodic object. They lie at distance $d_x = \frac{\lambda f_1}{d_{x_0}(2M+1)}$, $d_y = \frac{\lambda f_1}{d_{y_0}(2N+1)}$ from one another. The applied filter of spatial frequencies have to transmit only the higher peaks from the Fourier image of the finite periodic objects. The filter is a black mask with transmitting holes disposed at matched distances $\boldsymbol{d} = (d_x, d_y)$. Its transmittance is

$$t_f(x, y) = p(x, y) \otimes \sum_{m=-\infty}^{m=+\infty} \sum_{n=-\infty}^{n=+\infty} \delta(x - md_x, y - nd_y), \tag{3}$$

where $p(x, y)$ describes the transmittance of an individual hole in the mask.

The filter is situated in focal plane of the first lens L_1 of the coherent optical system.

The second lens formes the image

$$\hat{U}_{im}(x_1, y_1) \propto \sum_{-\infty}^{+\infty} \sum_{-\infty}^{+\infty} \hat{P}(md_{x_1}, nd_{y_1}) \times t_c(x_1 - md_{x_1}, y_1 - nd_{y_1}). \tag{4}$$

$|P(x_1, y_1)|^2 = |F\{p(x, y)\}|^2$ is a weighting factor in irradiance distribution. It modulates the brightness of the images. Individual pattern images are lying at the distances

$$d_{x_1} = \frac{f_2}{f_1} d_{x_0}, \quad d_{y_1} = \frac{f_2}{f_1} d_{y_0}.$$

By filtering out the respective spatial frequency the information about input dimensions of the periodical object is eliminated. However, the information about individual pattern transmittance remains fully restored in the image within the possibility of the optical system used. As it can be seen in condition for d_x, d_y formulated in eq. (3) the employed sampling of the Fourier spectrum corresponds to the Whittaker-Shannon sampling theorem for individual pattern t_c [1, 2]. On the other hand, transmission of the harmonic spatial frequencies enables to preserve information about input object dimensions.

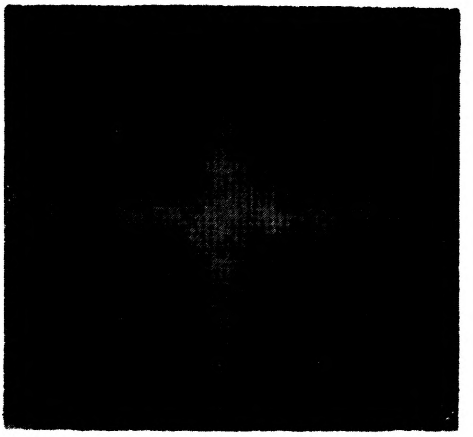

Fig. 3. Fourier image of finite periodic objects, 3× magnified

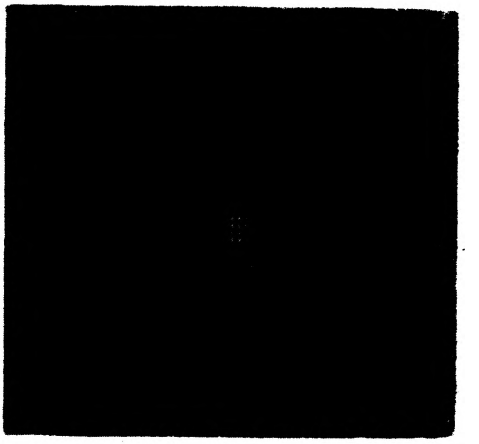

Fig. 4. The same through the matched mask, 3× magnified

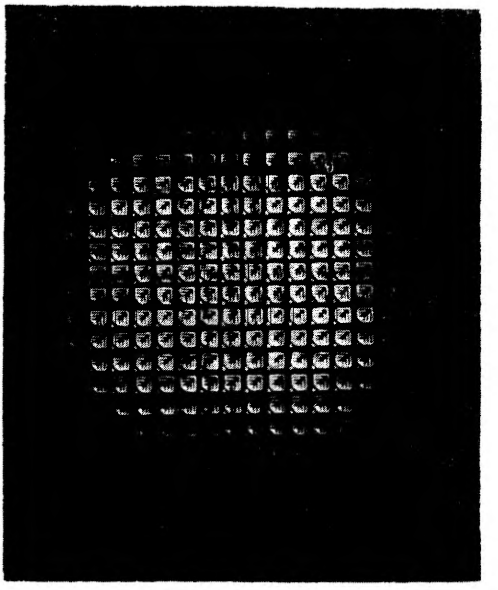

Fig. 5. Image resulting from the matched periodic filtering

Spatial frequency mask realized approximately according to eq. (3) must contain the holes as small as possible. Nevertheless in physical experiments they have definite (finite) sizes and shape. This fact will affect the image. For a circular hole with radius r_0, we have $p(x, y) = \mathrm{circ}\, r$, where

$$\mathrm{circ}\, r/r_0 = \begin{cases} 1, & r \leqslant r_0 \\ 0, & r > r_0 \end{cases}$$

and the image light field $\hat{U}_{im}(x_1, y_1)$ becomes

$$\hat{U}_{im}(x_1, y_1) \propto \sum_{-\infty}^{+\infty} \sum_{-\infty}^{+\infty} r_0 \frac{J_2(2\pi R r_0)}{R} t_c(x_1 - m d_{x_1}, y_1 - n d_{y_1}), \tag{5}$$

$r_0^2 J_1^2(2\pi R r_0) R^{-2}$ acts as a weighting factor on irradiance distribution, where $R^2 = (m d_{x_1})^2 + (n d_{y_1})^2$ and J_1 — the Bessel function of the first kind and order really masks the edges of filtering holes, whichever little they are, generates diffracted waves. Hence, the real hole shape introduces the above mentioned modulation of images irradiance. An extended image of a finite periodic pattern, obtained by matched spatial filtration, is shown in fig. 5. The mask transmitted only the principal peaks from the Fourier spectrum (see figs. 3 and 4). The holes in the mask used in our experiments had dimensions camparable with the peak breadth. Irradianee modulation of the extended image is then seen distinctly.

References

[1] SHANNON C. E., Proc. IRE **37** (1949), 10.
[2] LINDEN D., Proc. IRE **47** (1959), 1249.

Received January 25, 1980,
in revised form March 10, 1980

Optica Applicata, Vol. X, No. 4, 1980

On a possibility of the phase recovery from intensity distributions generated by differential operators in two-dimensional coherent imaging*

Piotr Kiedroń

Institute of Physics, Technical University of Wrocław, Wrocław, Poland.

It has been shown [1, 2] that the phase distribution in the image plane may be uniquely recovered from the intensity distributions at the input and output planes of some one-dimensional coherent differential operator. The most convenient physical realization of such an operator is to insert a transmittance of the form

$$T_1(u) = (2\pi i u)^n \tag{1}$$

into the exit pupil of an optical system before measuring the first intensity distribution $i_1(x)$ in the image plane. The second intensity measurement is performed after $T_1(u)$ is replaced with the transmittance

$$T_2(u) = (2A\cdot u+B)\,(2\pi i u)^n. \tag{2}$$

To reconstruct the complex amplitude $F(u)$ in the exit pupil it is sufficient to know the both intensity distributions $i_1(x)$, and $i_2(x)$, provided that the following inequality holds

$$|B/A| \geqslant 2u_0, \tag{3}$$

where u_0 is the cut-off frequency of the original complex amplitude $f(x)$ in the image plane before any differential filtering. In the two-dimensional case, however, information contained in the intensities $i_1(x, y)$ and $i_2(x, y)$ is not sufficient for unique phase reconstruction. In order to give an example of the possible phase ambiguity, let us examine the following complex amplitude of separated variables.

Let us consider a two-dimensional complex amplitude

$$F'(u, v) = F_1(u)\cdot F_2(v) \tag{4}$$

in the exit pupil before the transmittance $T_1(u)$ or $T_2(u)$ is introduced. Let us assume that the function

$$f_2(y) = \mathscr{F}\{F_2(v)\}, \tag{5}$$

where $\mathscr{F}$ denotes the Fourier transform, has at least one complex zero denoted by z_0. Then the both complex amplitudes

$$F''(u, v) = F_1(u)\mathscr{F}^{-1}\left\{f_2(y)\frac{y-z_0^*}{y-z_0}\right\}, \tag{6}$$

* This work was carried out under the Research Project M.R. I.5.

and $F'(u, v)$ generate the same intensity distributions in the image plane if the transmittance $T_2(u)$ is introduced. Since the transmittance $T_2(u)$ is independent of v, the complex amplitudes $F'(u, v)$ and $F''(u, v)$ produce the same intensity distributions in the image plane during the second measurement. The above property of the complex amplitudes (4) and (6) is in accordance with the Walther's theorem [3].

The phase ambiguity may be excluded if the additional third intensity measurement is performed. In order to obtain the unique phase recovery from three measurements in the two-dimensional case it is assumed that the transmittances

$$T_k(u, v) = (2A_k u + B_k)(2C_k v + D_k) \qquad \text{for } k = 1, 2, 3$$
$$\times (2\pi i u)^n (2\pi i v)^m \operatorname{rect}\left(\frac{u}{2u_0}\right) \operatorname{rect}\left(\frac{v}{2v_0}\right), \tag{7}$$

n, m being any nonnegative integers, are located in the exit pupil one after the other. The constants A_k, B_k, C_k, D_k are real and have the following properties

$$A_1 = C_1 = 0, \qquad B_1 = D_1 = 1, \tag{8a}$$
$$|B_2/A_2| \geqslant 2u_0, \qquad C_2 = 0,\ D_2 = 1, \tag{8b}$$
$$|D_3/C_3| \geqslant 2v_0, \qquad A_3 = 0,\ B_3 = 1. \tag{8c}$$

The intensity obtained in consecutive measurements ($k = 1, 2, 3$) takes the form

$$i_k(x, y) = |f_k(x, y)|^2, \tag{9}$$

where

$$f_k(x, y) = \int_{-\infty}^{\infty} du \int_{-\infty}^{\infty} dv F(u, v) T_k(u, v) \exp 2\pi i(ux + vy). \tag{10}$$

It has been assumed that the support of the function $F(u, v)$ (i.e. the area of the exit pupil) is contained within the rectangle $[-u_0, u_0] \times [-v_0, v_0]$.

Under the above assumptions (7)—(10) the unique recovery of the complex amplitude $F(u, v)$ is assured. The uniqueness is proved by simple reasoning given below.

By using the definitions (7), (8a), and (8b) and from equations (9) and (10) the intensity distribution in the first two measurements ($k = 1, 2$) may be written in the following form

$$i_1(x, y) = \left| \int_{-u_0}^{u_0} du F_y(u) (2\pi i v)^n \exp 2\pi i u x \right|^2, \tag{11a}$$

$$i_2(x, y) = \left| \int_{-u_0}^{u_0} du F_y(u) (2A_2 u + B_2)(2\pi i u)^n \exp 2\pi i u x \right|^2, \tag{11b}$$

where

$$F_y(u) = \int_{-v_0}^{v_0} dv F(u, v)\,(2\pi i v)^m \exp 2\pi i v y. \tag{12}$$

The formulae (11a) and (11b) are identical to the corresponding formulae in one-dimensional phase problem solved in [2] for any fixed y. Thus, $F_y(u)$ may be determined uniquely with the accuracy up to the constant (independent of the variable u) phase factor $\exp[ic'(y)]$ for any fixed y separately. It means that the left-hand side of the equation:

$$f_1'(x, y) = f_1(x, y)\cdot\exp[ic'(y)] \tag{13}$$

is known. By the same means, the intensities $i_1(x, y)$ and $i_3(x, y)$ may be expressed by the function

$$F_x(v) = \int_{-u_0}^{u_0} du F(u, v)\,(2\pi i u)^n \exp 2\pi i u x. \tag{14}$$

Analogically it may be shown that the complex amplitude

$$f_1''(x, y) = f_1(x, y)\exp[ic''(x)] \tag{15}$$

is also known. So far, however, the functions $c'(y)$ and $c''(x)$ have not been determined. Next we divide eq. (13) by the eq. (15) and fix the variable x (putting, for instance, $x = 0$) to obtain the following equation

$$\exp[ic'(y)] = \frac{f_1'(0, y)}{f_1''(0, y)} \exp[-ic''(0)]. \tag{16}$$

By this procedure the function $c'(y)$ has been determined with the accuracy to the additive constant component c. This is equivalent to the unique recovery of the complex amplitude $f_1(x, y)$ or $F(u, v)$ with accuracy up to the constant phase factor $\exp(ic)$.

It is easy to verify that the uniqueness is preserved if the first transmittance $T_1(u, v)$ is of the form

$$T_1(u, v) = (2A_2u+B_2)\,(2C_3v+D_3)\,(2\pi i u)^n\,(2\pi i v)^m \times \mathrm{rect}\left(\frac{u}{2u_0}\right)\mathrm{rect}\left(\frac{v}{2v_0}\right) \tag{17}$$

while $T_2(u, v)$ and $T_3(u, v)$ remain identical to those defined in (7), (8b), and (7), (8c), respectively.

It is worth noting that if $u_0 = v_0$, and $n = m$, it suffices to rotate the transmittance $T_2(u, v)$ by the angle equal to $\pi/2$ before the third measurement. The transmittances, for which the constants A_k, B_k, C_k, and D_k are selected in such a way that $T_k(u, v)$ are nonnegative within the whole domain, seem to be most useful, because of their easy production. This requires also the normalization of the transmittances, i.e. condition

$$|T_k(u, v)| \leqslant 1. \tag{18}$$

Despite the above restrictions the range of the possible variability of A_k, B_k, C_k, D_k is still wide. To impose the required properties on the applied algorithm a suitable choice of those constants may be needed. The paper concerning the application of the Gerchberg-Saxton-Misell algorithm [4, 5] to the method above proposed and the examination of its stability is being prepared.

References

[1] KIEDROŃ P., Optica Applicata **X** (1980), 149.
[2] KIEDROŃ P., Optica Applicata **X** (1980), 253.
[3] WALTHER A., Optica Acta **10** (1962), 41-49.
[4] GERCHBERG R. W., SAXTON W. O., Optik **35** (1972), 237-246.
[5] MISELL D. L., J. Phys. D: Appl. Phys. **6** (1973), L6-L9.

Received February 8, 1980

Optica Applicata, Vol. X, No. 4, 1980

On estimation of speckling pattern rotation caused by rotating object for small angles of rotation*

Wacław Urbańczyk, Ireneusz Wilk

Institute of Physics, Technical University of Wrocław, Wrocław, Poland.

Recently, the speckling interferometry has been intensively developed finding still new fields of applications. One of those fields is the measurement of small rotation angles by the method of double-exposure recording of the respective speckle pattern. For these reasons the knowledge of the correlation between the rotation angle of the speckling pattern and that of the rotated object surface becomes of importance. The estimation of this correlation is the subject of this letter.

This problem was considered in [1], for a special case when the direction of observation (recording) was perpendicular to the rotated object surface. Below, we shall discuss the general case of arbitrary orientations of incident beam, rotation axis and observation direction and prove that the formula derived in [1] preserves its validity. This result will be verified experimentally.

Theory

For the sake of convenience the ray directions will be determined by the respective angles made with the axis of the object rotation. Let P denote the plane perpendicular to the axis of rotation (fig. 1) and let an incident

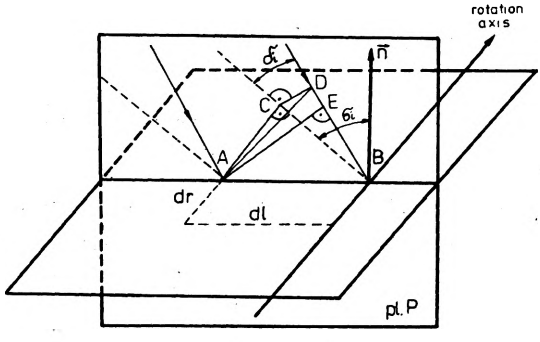

Fig. 1. Geometry of the setup for the incident beam

ray be projected perpendicularly onto this plane. Denote by σ_i the angle between the incident ray projection and the normal contained in the surface P, and by δ_i the angle between ray and its projection, respectively. The corres-

* This work was carried out under the Research Project M. R. I. 5.

ponding angles determining the direction of observation (recording) will be denoted by σ_o and δ_o. The angles chosen in this way are mutually independent, which means that a change of one of them is not necessarily associated with the change of the other. In particular the rotation of the object surface affects only the angles σ_i and σ_o leaving the others (i.e. δ_i and δ_o) unchanged.

In order to determine the change in angular position of the speckling pattern elements due to object surface rotation, let us first consider the phase distribution* in an elemental square of sizes dl and dr. It may be easily noted that the phase distribution along an arbitrary segment parallel to dr is determined only by δ_i angle, being not affected by the change of the angle σ_i which is due to the scattering surface rotation (as the angle between the direction of illuminating beam propagation and the segment dr remains unchanged). On the other hand, any change in angle σ_i causes some change in the phase distribution along the segments parallel to dl. The last change may be compensated by the respective change in the observation angle σ_o.

Let us calculate the optical path difference X_i of two rays incident at the ends of the segment dl. From fig. 1 we see that:

$$\begin{aligned}
AB &= dl,\\
AC &= dl\cos\sigma_i,\\
CB &= dl\sin\sigma_i,\\
CD &= dl\sin\sigma_i\tan\delta_i,\\
AD &= dl(\cos^2\sigma_i+\sin\sigma_i\tan\delta_i)^{1/2},\\
DB &= dl\sin\sigma_i/\cos\delta_i,\\
EB &= X_i.
\end{aligned}$$

From the triangle ABD we have immediately

$$X_i = EB = \frac{AB^2+BD^2-AD^2}{2BD}$$

$$= \frac{dl}{2}\left[\frac{\sin\sigma_i}{\cos\delta_i}+\frac{\cos\delta_i}{\sin\sigma_i}-\frac{(\cos^2\delta_i+\sin^2\sigma_i\tan^2\delta_i)\cos\delta_i}{\sin\sigma_i}\right] = dl\cos\delta_i\sin\sigma_i.$$

Analogically, the optical path difference for the rays travelling from the ends of the segment dl to the observation point at infinity may be estimated as

$$X_i = dl\cos\delta_o\sin\sigma_o.$$

Thus, the total optical path difference is equal to

$$\Delta = X_i - X_0 = dl(\cos\delta_i\sin\sigma_i-\cos\delta_o\sin\sigma_o).$$

---

* For the sake of simplicity we neglect here the microstructure (roughness) of the scattering object surface (which in reality creates the speckling pattern structure) being interested only in the changes of the speckling pattern position as determined by the respective changes in the geometry of the system occurring due to the object rotation

The change of the optical path difference due to the small rotation of the scattering surface, resulting in the respective changes $d\sigma_o$ and $d\sigma_o$ of the angles σ_i and σ_o as well as in the change $\Delta(dl)$ of the size dl, amounts to

$$d\Delta = dl[\cos\delta_i\cos\sigma_i d\sigma_i - \cos\delta_o\cos\sigma_o d\sigma_o] + \Delta(dl)\,[\cos\delta_i\sin\sigma_i,\ \cos\delta_o\sin\sigma_o].$$

However, the respective change $\Delta(dl)$ of dl being usually insignificant to the problem may be omitted*. Thus, finally

$$d\Delta = dl[\cos\delta_i\cos\sigma_i d\sigma_i - \cos\delta_o\cos\sigma_o d\sigma_o].$$

This change in the optical path will shift the speckling pattern to such a new angular position for which $\delta(d\Delta) = 0$. This requirement gives the following relation

$$d\sigma_o = \frac{\cos\delta_i\cos\sigma_i}{\cos\delta_o\cos\sigma} d\sigma_i. \tag{1}$$

Now, let the rotation angle be $d\beta$. Then $d\sigma_i = d\beta$ and $d\sigma_o = d\alpha - d\beta$, where $d\alpha$ denotes the rotation angle of the speckle primarily positioned at the original observation direction. Substituting these relation to (1) and noting that (see fig. 2)

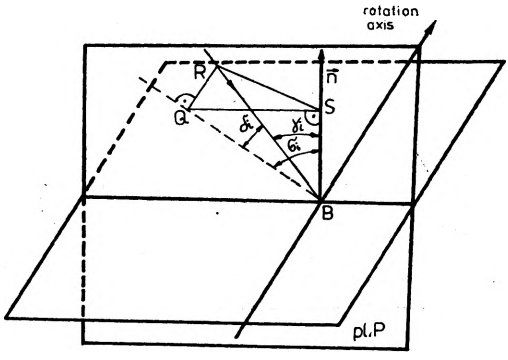

Fig. 2. Angular coordinates of the incident beam with respect to the scattering object surface

---

* The increase $\Delta(dl)$ in the size dl of an elemental scatterer results only in the respective increase of its area by the value $dr\cdot\Delta(dl)$. The light contribution from this additional area to any speckling pattern element may be considered to consist of the amplitude and phase parts, both of them being usually of the same statistical nature as those coming from the whole elemental scatterer area. Thus, the statistics of the scattered complex amplitude is preserved which, together with the fact that the area increment $dr\cdot\Delta(dl)$ is much smaller than the original scatterer area $dr\cdot dl$, makes the speckling pattern (being its Fourier spectrum) almost unaffected. This problem is in reality much more complex but its rigorous treatment is outside the scope of this letter.

$$\cos\delta_i = QB/RB,$$
$$\cos\sigma_i = SB/QB,$$
$$\cos\gamma_i = SB/RB$$

and, consequently, that $\cos\delta_i \cos\sigma_i = SB/RB = \cos\gamma_i$, we obtain after simple rearrangements

$$da = \left(1 + \frac{\cos\gamma_i}{\cos\gamma_o}\right) d\beta, \tag{2}$$

where γ_i is the angle of incidence of the illuminating beam and γ_o the angle of observation. Thus, the rotation of the speckle pattern da proved to be independent of the orientation of the object rotation axis with respect to both the illuminating beam and observation direction.

Experimental

The formula (2) has been verified approximately by using the geometry shown in fig. 3. The speckles were recorded at the photographic plate located at the distance 200 mm from the object, while the direction of

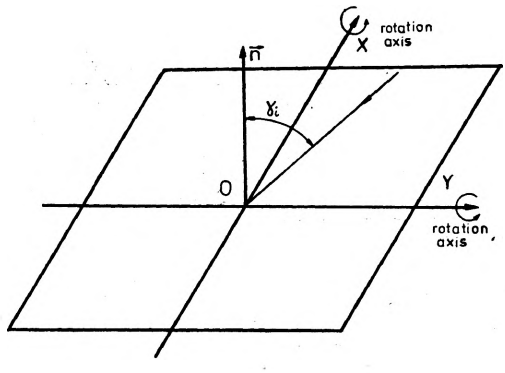

Fig. 3. The experimental setup used to measure the angle da of speckle pattern rotation, for the object rorated around the OX and OY axes, respectively

observation was normal to the scattering surface. The OX and OY axes were consecutively taken as the two different rotation axes. In this case the formula (2) is reduced to the form

$$da = (1 + \cos\gamma_i) d\beta.$$

The experimental results have been collected in the table.

The consequences of the above results to the measurement of small rotations by the method of free propagation speckling will be the subject of the next paper.

Table

Rotation angle d of the scattering surface the same for the rotations around the OX and OY axes	Calculated rotation angle da of the speckles	Measured rotation angles da for the speckles	
		For the OX axis	For the OY axis
$\gamma_i = 73°$; $(1+\cos 73°) = 1.292$			
0.00025	0.00032	0.00029	0.00025
0.00050	0.00065	0.00057	0.00069
0.00075	0.00097	0.00112	0.00085
0.00100	0.00129	0.00132	0.00140
0.00125	0.00162	0.00153	0.00178
$\gamma_i = 55°$; $(1+\cos 55°) = 1.573$			
0.00025	0.00039	0.00032	0.00040
0.00050	0.00079	0.00085	0.00073
0.00075	0.00118	0.00115	0.00128
0.00100	0.00157	0.00153	0.00169
0.00125	0.00197	0.00215	0.00183
$\gamma_i = 25°$; $(1+\cos 25°) = 1.906$			
0.00025	0.00048	0.00042	0.00056
0.00050	0.00095	0.00105	0.00083
0.00075	0.00143	0.00140	0.00187
0.00100	0.00190	0.00207	0.00187
0.00125	0.00238	0.00250	0.00241

References

[1] Gregory D. A., Optics and Laser Techn. 8 (1976), 201.

Received March 5, 1980

Optica Applicata, Vol. X, No. 4, 1980

Flashlamp excited tuned dye laser

Zdzisław Konefał, Jan Szczczepański

Institute of Physics, University of Gdańsk, ul. Wita Stwosza 57,
80-952 Gdańsk, Poland

Dye laser have found numerous applications in research and technology because of their unique properties. Flashlamp pumping of a laser not only simplifies its construction but also makes possible a generation of high-power pulses.

The present work concerns a narrow-band tuned dye laser pumped with air-filled flashlamps. The laser design and performance curves are presented.

Schematic diagram of the laser head is shown in fig. 1. So-called dense poching with aluminium foil was used. *O*-ring seals make the system tight and facilitate the lamp replacement in a case of damage. High repetition rate can be achieved by water-cooling of the lamps.

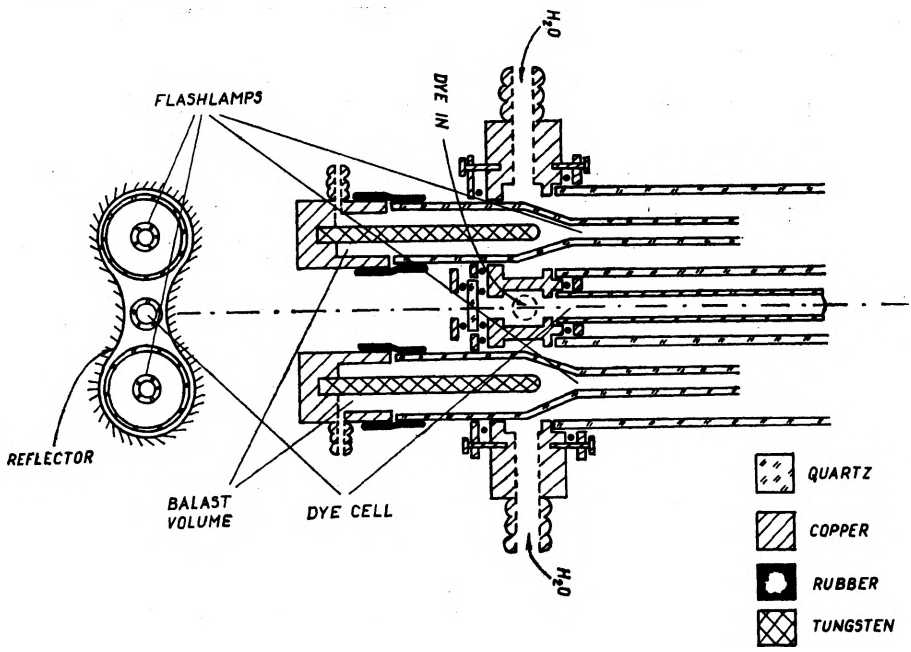

Fig. 1. Cross-section of the laser head

To make the lamp more resistant to shock waves a flexible connection to the electrode with a rubber band and a ballast space were adopted [1, 2].

Tungsten tips of the electrodes reduce their sputtering. The air is pumped out of the lamp by a rotary pump connected to one of the electrodes through a connecting piece.

To ensure the high efficiency of lasing in a dye laser, losses due to the triplet-triplet absorption should be reduced by using short pumping pulses [3]. The shape of the exciting pulse depends highly on the electric connections between the lamp and the capacitors. Two kinds of arrangement, as shown in fig. 2, namely the classical circuit and the Blumlein-

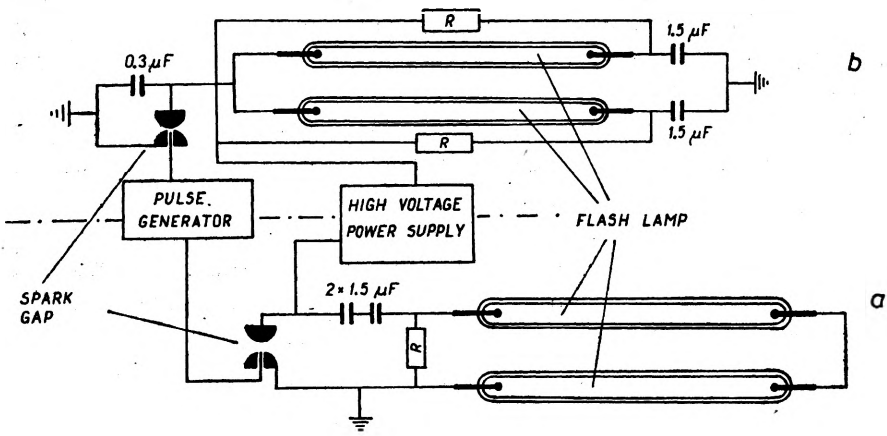

Fig. 2. Electric circuit diagrams
[a) classical connection of lamps and capacitors, b) Blumlein-type circuit

type circuit were used [4]. Flashlamp light outputs obtained with the circuits are shown in fig. 3. It can be seen that the flash half-time for the Blumlein-type circuit was equal to 500 ns, being thus three times less than that for the classical circuit.

The relative laser output energy was measured as a function of the electric energy stored in the capacitors. The results are shown in fig. 4. Solution of 7-methylcoumarin in ethanol was used as working medium of the laser. The optimum pressure of 14 HPa was kept in the flashlamps. Fig. 5 shows a relative laser output energy as a function of the gas pressure in the flashlamps. In this case the energy increases monotonically with the pressure to reach the maximum at about 14 HPa.

It follows from the measurements that the effective operation of the dye laser requires that the working medium be kept at the same temperature as that of the water cooling the lamp. If these temperatures are not equal the respective temperature gradient in the working medium

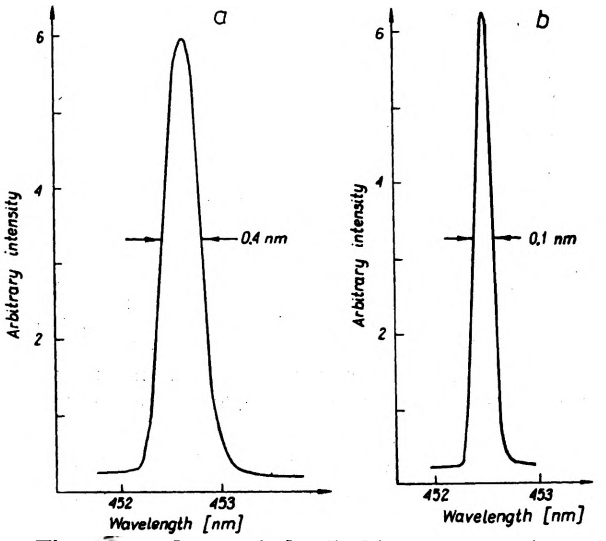

Fig. 3. Time dependence of the flashlamp output intensity
a) for the classical circuit, b) for the Blumlein-type circuit

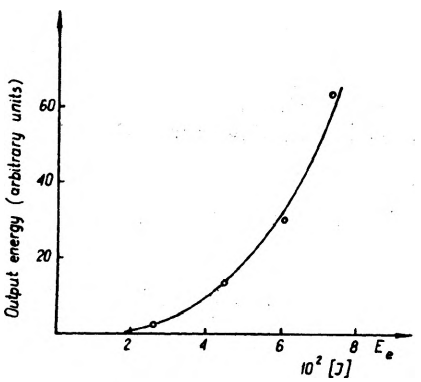

Fig. 4. Relative laser output energy as a function of electric energy stored in the capacitors (Blumlein-type circuit)

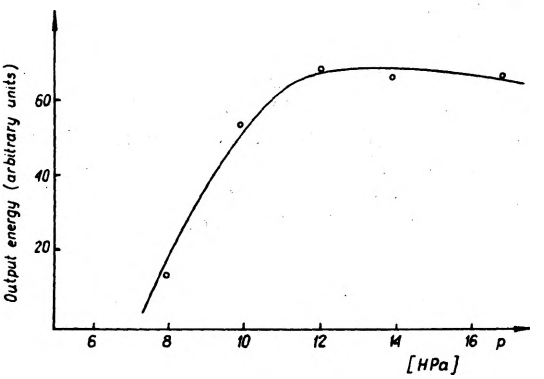

Fig. 5. Relative laser output energy as a function of the gas pressure

will reduce substantially the lasing efficiency. To avoid this effect a special cooling system of the working medium was used.

Two Fabry-Pérot interferometers were placed inside the laser cavity to obtain a narrowed laser output spectrum [5]. Plates in these interferometers were placed apart 5 μm and 150 μm, respectively. Output beam bandwidths obtained inside the cavity with one and two interferometers are shown in fig. 6. With two interferometers the spectral width amounted to 0.1 nm.

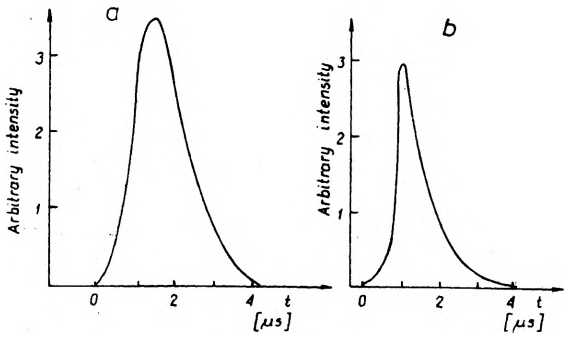

Fig. 6. Output frequency spectrum
a) with one interferometer inside the cavity, b) with two interferometers

The laser described in this report has been applied to a remote detection of atmospheric constituents using a difference absorption method (LIDAR).

Acknowledgements — The authors wish to thank Prof. J. Heldt for helpful discussions.

References

[1] OKADA T., et al., Appl. Phys. **15** (1978), 191.
[2] EFTHYMIOPOULS T., GARSIDE B. K., Appl. Opt. **16** (1977), 70.
[3] SCHÄFER J.F.P. Ed., *Dye Laser*, Springer-Verlag, Berlin, New York, Heidelberg, 1973.
[4] BERGMAN E.E., Appl. Phys. Lett. **28** (1976), 84.
[5] BRADLEY D.I., et al., IEEE J. Quantum Electron., QE-4. 707, 1968.

Received May 31, 1980